Sentinel-2 image capacities to predict common topsoil properties of temperate and Mediterranean agroecosystems

Emmanuelle Vaudour, Cécile Gomez, Youssef Fouad, Philippe Lagacherie

SENTINEL-2 image capacities to predict common topsoil properties of temperate and Mediterranean agroecosystems

E. Vaudour[1]*, C. Gomez[2], Y. Fouad[3], P. Lagacherie[4]

[1]UMR ECOSYS, AgroParisTech, INRA, Université Paris-Saclay, 78850, Thiverval-Grignon, France *Email: Emmanuelle.Vaudour@agroparistech.fr

[2] IRD, UMR LISAH (INRA-IRD-SupAgro), F-34060 Montpellier, France

[3]UMR SAS, Agrocampus Ouest, INRA, 35042, Rennes, France

[4] INRA, UMR LISAH (INRA-IRD-SupAgro), F-34060 Montpellier, France

Abstract

To be fully operational for facilitating decisions made at any spatial level, models and indicators of soil ecosystem functions require the use of precise spatially referenced soil information as inputs. This study aimed at exploring the capacity for SENTINEL-2A (S2A) multispectral satellite images to predict several topsoil properties in two contrasted pedoclimatic environments: a temperate region marked by intensive annual crop cultivation patterns and soils derived from loess or colluvium and/or marine limestone or chalk (Versailles Plain, 221 km^2); and a Mediterranean region marked by vineyard cultivation and soils derived from lacustrine limestone, calcareous sandstones, colluvium, or alluvial deposits (Peyne catchment, 48 km^2). Prediction models of soil properties based on partial least squares regressions (PLSR) were built from S2A spectra of 72 and 143 sampling locations across the Versailles Plain and Peyne catchment, respectively. Eight soil surface properties were investigated in both regions: pH, cation exchange capacity (CEC), texture fractions (Clay,

Silt, Sand), Iron, Calcium Carbonate ($CaCO_3$) and Soil Organic Carbon (SOC) content. Predictive abilities were studied according to the root mean square error of cross-validation (RMSECV) tests, cross-validated coefficient of determination (R^2_{cv}) and ratio of performance to deviation (RPD). Intermediate prediction performance outcomes (R^2_{cv} and RPD greater than or equal to 0.5 and 1.4, respectively) were obtained for 4 topsoil properties found across the Versailles Plain (SOC, pH, $CaCO_3$ and CEC), and near-intermediate performance outcomes ($0.5 > R^2_{cv} > 0.39$, $1.4 > RPD > 1.3$) were yielded for 3 topsoil properties (Clay, Iron, and CEC) found across the Peyne catchment and for 1 property (Clay) found across the Versailles Plain. The study results show what can be expected from SENTINEL2 images in terms of predictive capacities at the regional scale. The spatial structure of the estimated soil properties for bare soils pixels is highlighted, promising further improvements made to spatial prediction models for these properties based on the use of Digital Soil Mapping (DSM) techniques.

Key words: soil properties, SENTINEL-2A, partial least squares regression, temperate soils, Mediterranean soils, agroecosystems.

1. Introduction

Soils carry out a number of key environmental functions that are essential for human subsistence (e.g., food, fiber and timber production, water storage and redistribution, pollutant filtering and carbon storage). The understanding and modeling of physical, chemical and biological processes underlying these different functions have been the subject of many scientific works now that a number of models or indicators that represent these functions are available (Sanchez et al., 2009; Adhikari and Hartemink, 2016; Baveye et al. 2016). To be fully operational in facilitating decisions made at local, national and global levels, these

models and indicators require the use of precise spatially referenced soil information as inputs.

Given the lack of precision and extension of existing soil databases, Digital Soil Mapping (Mc Bratney et al., 2003) methods have been recognized as the most adequate and operational response to these requirements (Arrouays et al., 2014, Minasny & McBratney, 2016). However, even though digital soil maps of soil properties are now being produced across the globe (Arrouays et al., 2017) and for large areas—regions, countries and even continents—at high resolutions (100 m), they still provide very uncertain estimations of soil properties due to the limited availability of sites offering soil property measurements used for calibrating DSM models (Vaysse et al., 2015).

Visible, Near-infrared and Short-wave Infrared (VNIR/SWIR) hyperspectral remote sensing methods have been demonstrated to serve as promising means to significantly increase the number of sites offering quantitative estimations of topsoil properties (e.g., Soil Organic Carbon (SOC), pH, Cation Exchange Capacity (CEC), texture fractions (clay, silt, sand), Iron and Calcium Carbonate ($CaCO_3$)) (e.g., Selige et al., 2008; Stevens et al., 2010; Gomez et al., 2012; Vaudour et al., 2016). For bare soil surfaces, accurate local estimates ($R^2_{cv} > 0.7$) have been obtained for soil properties i) related to a chemical species that impacts soil surface reflectance values through absorption bands (e.g., OH- ion for clay) (Ben-Dor et al., 2002) or ii) highly correlated with the latter (e.g., CEC with clay content) (Ben-Dor et al., 2002), iii) showing a sufficient level of variability across study regions (Gomez et al., 2012a & b). For instance, Selige et al. (2006) mapped SOC content, a soil property having specific spectral behaviour and high spatial variability over their study area. In addition, they also mapped Total Nitrogen, a soil property deprived of specific spectral features but, due to an associated chemical or physical structure, correlated to a soil property having such features (being SOC). DSM approaches are designed to employ this new source of soil data to allow

for the exhaustive mapping of surface (Walker et al., 2017) and subsurface (Lagacherie et al., 2013) properties.

Although hyperspectral VNIR/SWIR imagery has been proven to serve as a valuable tool for mapping key soil surface properties, it cannot be applied for large surface mapping or for temporal monitoring because it is expensive to apply and because hyperspectral VNIR/SWIR imaging data are not widely available. Indeed, only one hyperspectral VNIR/SWIR satellite sensor is currently operational. The HYPERION sensor offers a spatial resolution of 30 m, a spectral resolution of 10 nm and a swath of 7.5 km (Folkman et al., 2001). Other hyperspectral VNIR/SWIR imaging sensors are airborne sensors (e.g., the Hymap, AISA-DUAL and HySpex sensors) with spectral resolutions of 5 to 10 nm, spatial resolutions of approximately 4-5 m (depending to the flight altitude) and flight prints of generally less than 400 km² (depending to the studied case). Furthermore, few studies have obtained successful results in terms of mapping soil properties from VNIR-SWIR multispectral satellite imagery that allow one to capture a larger area from a single nearly instantaneous glance (e.g., Vaudour et al., 2013; Shabou et al., 2015). This can be attributed to i) the low revisit frequency of sensors, which compromises the acquisition of images under clear conditions, while time ranges of bare soil availability, and particularly for annual crop systems, are short and ii) the coarse spectral and spatial resolutions of most historical multispectral sensors, which limit prediction performance outcomes (Gomez et al, 2015; Adeline et al., 2017).

The recent release of multispectral satellite SENTINEL-2A data by the European Space Agency last November 2015 is revolutionary in developing images of large areas with a 290 km-swath width at high revisit frequencies (planned to be near-daily when the full satellite constellation is in orbit). The multispectral SENTINEL-2A satellite provides 13

spectral bands at spectral resolutions of between 20 and 180 nm and at spatial resolutions of 10 to 60 m (§2.3).

The objective of this study is to assess the potential for SENTINEL-2A data to produce estimations of topsoil properties for large sets of sites. The study focuses on two French regions—the Versailles Plain and the Peyne Valley—that represent very different agroecosystems and that have both been previously used as test areas for topsoil mapping from VNIR/SWIR hyperspectral data (Vaudour et al, 2016 and Gomez et al, 2012, respectively).

2. Materials

2.1 Study areas

2.1.1 Versailles Plain

The Versailles Plain is an agricultural peri-urban region of 221 km² located west of Paris (North of France) that is characterized by intensive annual crop cultivation across an area of ~99 km² (Fig. 1, left). The main crop rotations in the area involve winter wheat, winter rapeseed, winter and spring barley and maize on occasion (Vaudour et al., 2015). Cultivation practices are mainly conventional, with early winter plowing applied at least 1 year out of every 3. The Versailles Plain is composed of two plateaus levels: one at a 120-m elevation in the center (lower limestone plateau) and another at a 170 m-elevation along the northern and southern edges of the area (upper millstone clay plateau). Both are oriented in the NW-SE direction toward the Palace of Versailles. Quaternary loessic deposits and loessic colluvium leave a mark on all landforms in the area and particularly on local plateaus, which have evolved into haplic or glossic luvisols according to the FAO classification (World Reference Base (WRB) (Crahet, 1992; Vaudour et al., 2013, 2014). The largely forested upper plateau

125 flanks are characterized by Fontainebleau acid sands that give rise to arenic cambisols, while
126 the lower plateau flanks, which are largely cultivated, are composed of calcaric cambisols
127 derived from limestone, colluvial materials and, along the lower slopes, chalk. Throughout the
128 lower slopes and valleys, stagnic colluvic cambisols are derived from marls or alluvio-
129 colluvial materials.
130

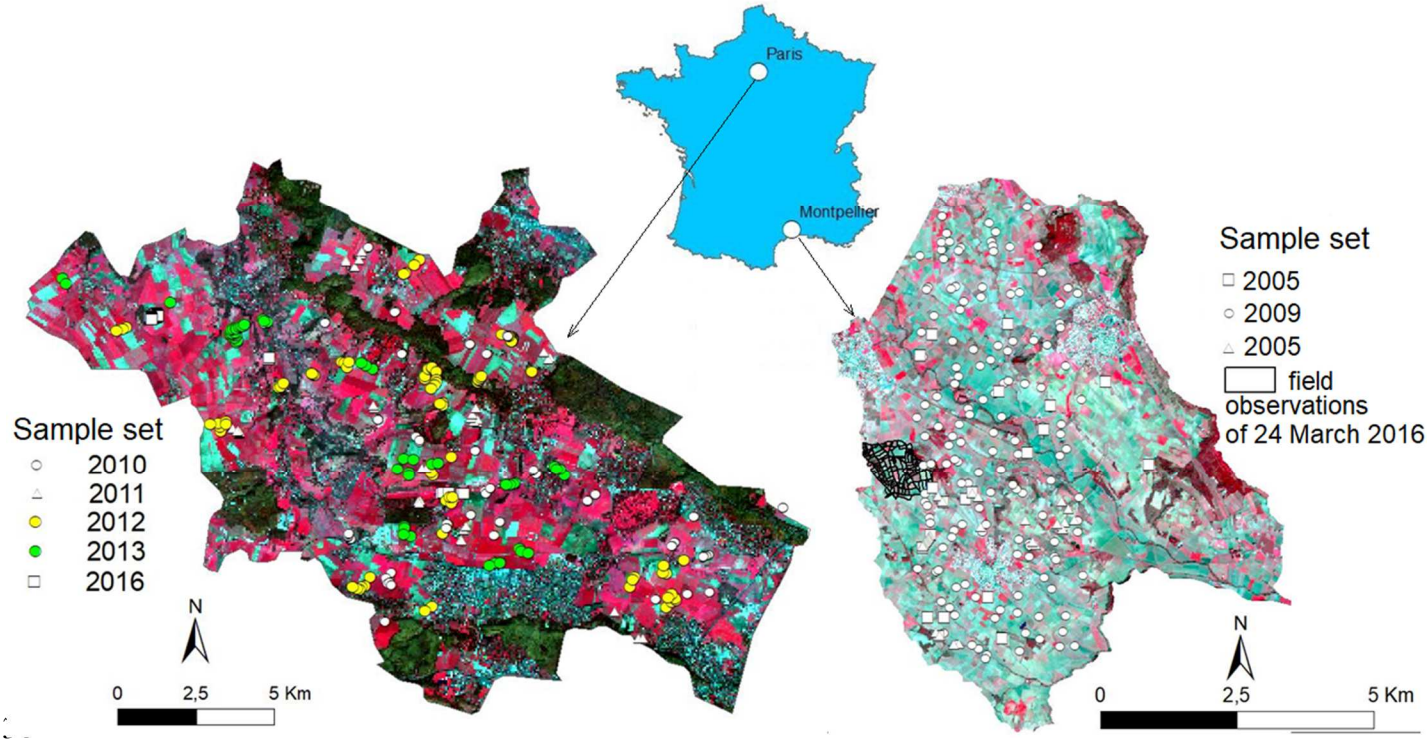

132 Figure 1. Locations of soil samples from the Versailles Plain (left, infrared colored S2A
133 image from 12 March 2016) and the lower Peyne Valley (right, infrared colored S2A image
134 from 19 March 2016), ©ESA 2016
135
136 2.1.2 La Peyne Valley
137 The lower valley of the Peyne River is a viticultural region of 48 km² located west of
138 Montpellier (South of France) (Fig. 1, right) and characterized by Plio-Quaternary alluvial
139 terraces and fan terraces, the deposits of which have undergone fersiallitization and which

have evolved into red Mediterranean soils or chromic luvisols (Coulouma, 2008). The valley base has been composed of marine Miocene sediments (marl, sandy loam, and calcareous sandstone) and marine Pliocene marl refillings since the Messinian salinity crisis. Gently undulating forms of hills and colluvial fans characterize landscape units in the area and give rise to several types of soils rich in calcium carbonate with a loamy sand texture and increasing clay levels toward the bases of the hillslopes: calcaric leptosols, calcaric regosols, and calcisols. A cuesta that characterizes the landscape unit has formed on lacustrine limestone of the Upper Miocene, where calcisols and calcaric regosols have developed with irregular bedrock depths creating variations in stoniness and calcium carbonate content levels. Alluvial terraces and alluvio-colluvial fans originating from Plio-Quaternary clays and alluvial deposits correspond to deep stony decarbonated chromic and/or colluvial luvisols, fluvisols, and some endogleyic calcisols. While early Quaternary terraces of the Peyne River have produced stony and clayey chromic luvisols, newer terraces have balanced textured fluvisols with carbonate content.

2.2 Soil samples and ground observations

2.2.1 Soil sampling

This study gathered two soil data sets that were collected for the purpose of earlier studies (for Versailles, Vaudour et al. 2013, 2014a, 2016; for La Peyne, Gomez et al, 2012). Despite some differences in chemical analysis, it was found useful to gather them in view of enlarging the range of the tested pedological situations. A total of 72 and 143 topsoil samples were collected from the Versailles Plain and Peyne Valley, respectively (Fig. 1). For the Versailles Plain, 69 topsoil samples were collected from 2010 to 2013, and 13 topsoil samples were collected in 2016. All of the samples were composed of roughly 10 sub-samples collected to a depth of 8 cm from random locations within a 2.7 × 2.7 m square area centered at the

165 sampling plot as recorded at its center using a Trimble Pathfinder®Power DGPS of 50 cm
166 precision (Vaudour et al., 2014). From the Peyne Valley, 39 topsoil samples were collected in
167 2005, and 104 topsoil samples were collected in 2009. All of the samples were composed of
168 five sub-samples collected to a depth of 5 cm from random locations within a 10 × 10 m
169 square centered on the geographical position of the sampling plot as recorded by a Garmin
170 GPS instrument.
171
172
173 2.2.2 Physico-chemical analysis
174 Topsoil samples collected from both study areas were air-dried and then crushed and sieved to
175 2 mm. Soil property determinations were performed through a classical physico-chemical
176 analysis (Baize and Jabiol, 1995). In total, 8 common soil properties were considered for
177 spectral modeling (Table 1): content of 3 particle sizes or granulometric fractions of 2 mm-
178 sieved fine earth (total silt, 2 - 50 µm; total sand, 50 µm - 2 mm and clay, < 2 µm); calcium
179 carbonate ($CaCO_3$) content; free iron content (Mehra-Jackson); soil organic carbon (SOC)
180 content; pH; and cation exchange capacity (CEC).
181 Granulometric fractions (clay, silt, and sand) and $CaCO_3$ content levels were measured
182 from 143 soils samples collected from the Peyne Valley (Table 1). The three other soil
183 properties (iron, CEC and pH) were measured from 104 soil samples collected from the Peyne
184 Valley. For the Versailles Plain, all soil properties except for CEC (39 samples) were
185 measured (Table 1).
186
187 Table 1. Soil datasets used for models and statistics on soil properties

Soil property	Description	Unit	Versailles Plain						Peyne Valley					
			Sample size	Min	Q1	Median	Q3	Max	Sample size	Min	Q1	Median	Q3	Max
SOC	soil organic C	$g.kg^{-1}$	72	7.0	12.5	15.9	20.1	31.9	104	4.0	7.0	8.9	11.4	21.8

	content													
$CaCO_3$	total $CaCO_3$ content	$g.kg^{-1}$	72	0	0	27.1	67.2	530	143	0	22.2	136.0	251.0	473
Clay	granulometric fraction <2 µm	$g.kg^{-1}$	72	132	192.5	249.5	281.0	391	143	67	185.0	231.0	290.5	452
Silt	granulometric fraction 2-50 µm	$g.kg^{-1}$	72	228	474.8	542.0	603.0	774	143	141	252.0	322.0	384.5	655
Sand	granulometric fraction 50 µm – 2 mm	$g.kg^{-1}$	72	17	87.8	157.5	209.0	512	143	106	364.5	433.0	516.0	737
Iron	« free iron » content	g/100 g	72	0.51	0.75	0.87	0.97	1.29	104	0.03	0.75	1.07	1.58	2.92
pH	water-pH	-	72	5.61	6.91	7.99	8.18	8.34	104	5.37	8.3	8.46	8.54	8.70
CEC	cation exchange capacity	$cmol.kg^{-1}$	39	6.1	11.0	17.1	22.1	28.3	104	6.1	8.3	10.7	12.9	19.1

188

189

190 2.2.3 Ground observations

191 For the Versailles Plain, soil surface conditions were observed on 15 and 17 March 2016
192 across 6 agricultural fields and for other fields planned for spectral measurements. For the
193 Peyne Valley, vineyard soil surface conditions were observed on 24 March 2016 across the
194 0.9 km² sub-catchment of Roujan, which includes 75 viticultural fields. These observations
195 enabled us to define the threshold of the vegetation index for retrieving bare soil pixels from
196 S2A images. At the time that the images were acquired, the budburst stage had just begun for
197 vines in the Peyne Valley, and hence vine vegetation had not yet developed. For the
198 Versailles Plain, spring barley sowing had just started and maize and pea sowing had not
199 started, hence allowing for the observation of bare soils used for spring crops. For both study
200 areas, winter crops and grasslands were photosynthetically active and covering, and thus
201 easily identifiable and removable by means of NDVI.

202

203 *2.3 Remotely sensed images and geographic data*

204 Two SENTINEL-2A (S2A) images were acquired under nearly clear conditions on 12 and 19
205 March 2016 from the Versailles Plain and Peyne Valley, respectively (Table 2). The

multispectral instrument aboard the S2A satellite has 13 spectral bands, including 4 bands of a 10 m resolution and 6 bands of a 20 m resolution (Table 3) retained for spectral modeling. Both images were atmospherically corrected using the ATCOR2/3 radiative transfer model (Richter and Schläpfer, 2016).

Both study sites are characterized by urban activity and by the presence of bare soil, water and vegetation. To mask no-soil pixels from the S2 data, the following approach was applied. First, urban and water areas were masked using Land Parcel Registry maps. In turn, only cropland and vineyards were maintained across the study areas. Second, pixels with normalized difference vegetation index (NDVI) values exceeding an expert-calibrated threshold were masked. A value of 0.35 was determined for both sites after considering field observations (section 2.2.3). The NDVI was retrieved using bands of 842 nm and 665 nm. Finally, bare soils of the Versailles Plain represent 8.05% of our study area and 44,979 S2A pixels, while bare soils of the Peyne catchment represent 38.6% of our study area and 46,971 S2A pixels.

Table 2. Main characteristics of the studied scenes

Imaging date	Sensor	Output resolution (m)	Time of acquisition (U.T GMT)	Viewing incidence angle (°)	Sun azimuth (°)	Sun elevation (°)
12 March 2016	S2A	20	10:50:37	<5.1	160.5	36.1
19 March 2016	S2A	20	10:40:32	<3.3	157.6	43.7

Table 3. Characteristics of the Multi-Spectral Instrument aboard the SENTINEL2 satellite. Spectral S2A bands used are shown in bold.

Spectral band	Spatial resolution (m)	Central wavelength (nm)	Band width (nm)
b1	60	443	20
b2	**10**	**490**	**65**
b3	**10**	**560**	**35**
b4	**10**	**665**	**30**
b5	**20**	**705**	**15**
b6	**20**	**740**	**15**
b7	**20**	**783**	**20**
b8	**10**	**842**	**115**
b8A	**20**	**865**	**20**
b9	60	945	20

b10	60	1380	30
b11	**20**	**1610**	**90**
b12	**20**	**2190**	**180**

A selection of various reflectance spectra comprising the darkest and the brightest soils is shown in Fig. 2. The brightest soils comprise: (i) calcic or calcaric sandy soils originating from calcareous sandstone (La Peyne); (ii) silt-loam luvisols (Versailles) or eluviated horizons of the chromic luvisols (La Peyne), developing a slaking crust ; (iii) rendzic or calcaric cambisols with very high topsoil calcium carbonate content or outcropping underlying chalk (Versailles). The darkest soils are clayey and alluvial and, for Versailles, can have high organic carbon content (>20 g kg−1) and/or high roughness dating from late winter ploughing. Intermediate soil spectra comprise soils with either moderate rock fragment content (10–25%), or varied textures and intermediate to low roughness (both regions), and also red Mediterranean soils (La Peyne).

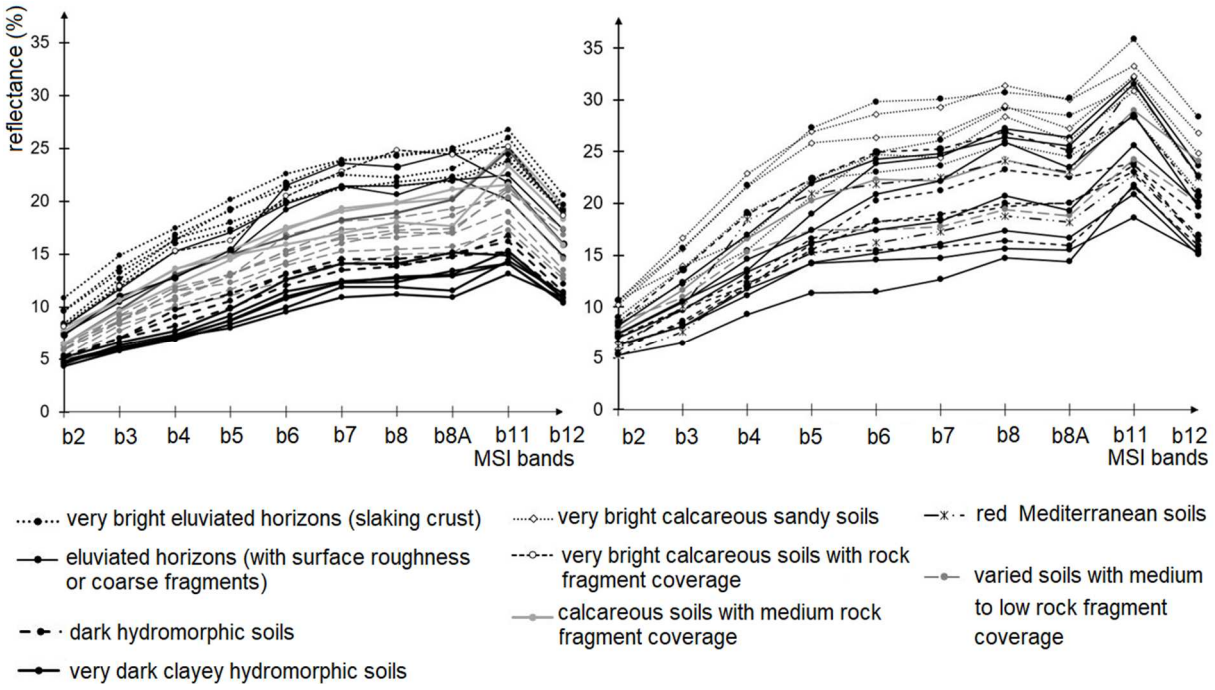

Figure 2. Selection of reflectance image spectra covering the whole dataset reflectance range and the main soil types

3. Methods

241 *3.1 Models for soil property prediction*

242 The partial least squares regression (PLSR) method was used to construct prediction models
243 based on bare soil samples drawn from each study region. The PLSR method relates two data
244 matrices, the matrix of explanatory variables X (here the soil spectra) and the matrix of
245 dependent variables Y (here the soil properties), through a linear multivariate model, but it
246 extends beyond traditional regression methods in that it also models the structures of X and Y
247 (Geladi and Kowalski, 1986; Wold et al., 2001). For Y in particular, PLSR extracts
248 orthogonal or latent predictor variables accounting for variation in the dependent variable.
249 The PLSR approach enables one to analyze data based on several noisy collinear features
250 (Wold et al., 2001), and it has been used widely for hyperspectral remote sensing (e.g., Selige
251 et al., 2008; Stevens et al., 2010; Gomez et al., 2012; Vaudour et al., 2016).

252 Prior to PLSR modeling, in order to maximize the fitting of target values against spectra, a
253 series of transforms were tested for either spectra or target values. Reflectance values of the
254 whole spectra were centered. For the Versailles Plain, Clay, SOC and $CaCO_3$ content levels
255 and CEC were log-transformed, while for both areas, the square root of iron content was used.
256 For La Peyne, log-transform of target values was not retained, as it did not bring any
257 improvement of the fitting. Outliers were detected for sets of image spectra or for sets of
258 measured soil properties. This was based on the 5% threshold of the standardized
259 Mahalanobis distance (Mark and Tunnel, 1985) and on the multivariate outlier detection
260 approach elaborated by Filzmoser et al. (2005). Outliers selected through both approaches
261 were retained as outliers.

262 For each target soil property Y, a PLSR model was constructed from preprocessed image
263 spectra with 10 selected spectral bands (Table 3). The optimal number of latent variables was
264 determined from the prediction residual error sum of squares (PRESS). Due to the limited
265 number of bare soil samples available, and because this study was more focused on

266 comparing performance levels between regions than on carrying out external validation
267 assessments, a leave-one-out cross-validation procedure was applied (Wold, 1978; Gomez et
268 al., 2012). The quality of model fit was evaluated from the root mean squared error of cross-
269 validation (RMSECV), from the coefficient of determination of cross-validation (R_{cv}^2) and
270 from the residual prediction deviation (RPD), i.e., the ratio between the standard deviation of
271 the calibration dataset to the RMSECV. According to Chang et al. (2001) and Viscarra-Rossel
272 et al. (2006), values of 1.4 to 1.8 denote models exhibiting moderate levels of predictive
273 capacity; values of between 1 and 1.4 denote models exhibiting poor levels of predictive
274 capacity, and values of <1 denote very poor models that should not be used.
275 PLSR models were used through R version 3.2.1 (R Development Core Team, 2015)
276 employing the "pls" package (Mevik and Wehrens, 2007).
277
278 *3.2 Variograms of predicted soil properties*
279 For the best predicted soil properties, PLSR models were applied to pixels of bare agricultural
280 soil. The spatial structure of the predicted pixels was examined and compared with that of
281 measured properties for the same locations. Spatial structures can be described from a
282 variogram that relates the spatial dependence or semi-variance between points at a distance of
283 h, i.e., the average variance between any pair of sampling points (Goovaerts, 1997):
284 $$\gamma(h) = \frac{1}{2n}\sum_{i=1}^{n}\{p(x_i) - p(x_i + h)\}^2 \quad (1)$$
285 where $\gamma(h)$ is the average semi-variance of the soil property, n is the number of pairs of
286 sampling points, p is the value of the property P, x is the coordinate of the point, and h is the
287 distance between pairs or the lag value.
288 For each best predicted soil property, two empirical variograms were built from
289 equation (1): the first was built from 143 or 104 values of the soil samples measured by
290 physico-chemical analysis; the second was built from predicted values for the same locations.

Simple omnidirectional variograms were calculated, and following Gomez et al. (2012), the spherical or exponential model used was fitted through a weighted least squares procedure (Pebesma, 2004) using the R statistical software program and the Gstats package. The universality condition (no drift) was assumed.

For the Versailles Plain, it was not possible to obtain experimental variograms suitable for fitting a model due to the limited number of sites involved and the clustered sampling scheme employed. Variograms were therefore only examined for the Peyne Valley. To examine the robustness of spatial structures at the scale of the entire study region, variograms were calculated from all bare soil pixels.

4. Results

4.1 Description of soils samples

Basic statistics on all of the soil properties measured are shown in Table 2. For the Peyne Valley, the range of clay contents present is higher than that of the Versailles Plain, with the highest value recorded as 452 $g.kg^{-1}$, though the 1st quartile and median values (185.0 and 231.0 $g.kg^{-1}$) are slightly lower than those for the Versailles Plain (192.5 and 249.5 $g.kg^{-1}$), while the 3rd quartile is slightly higher (290.5 $g.kg^{-1}$) than that for the Versailles Plain (281 $g.kg^{-1}$). SOC, silt and CEC levels are measured within a narrower and lower range for the Peyne Valley and with a much lower median (SOC, 8.92 $g.kg^{-1}$; silt content, 322 $g.kg^{-1}$; CEC, 10.65 $cmol+.kg^{-1}$) than that for the Versailles Plain (SOC, 15.9 $g.kg^{-1}$; silt content, 542 $g.kg^{-1}$; CEC, 17.10 $cmol+.kg^{-1}$). Conversely, sand and calcium carbonate content levels are higher in the Peyne Valley, with a higher median (sand content, 433 $g.kg^{-1}$; calcium carbonate content, 136 $g.kg^{-1}$) than that for the Versailles Plain (sand content, 157.5 $g.kg^{1}$; calcium carbonate content, 27 $g.kg^{-1}$). Consequently, pH values are higher and less variable for the Peyne Valley, while soils of the Versailles Plain vary more in terms of pH levels. Red Mediterranean

soils resulting from geochemical weathering contain more free iron, and hence their presence has induced a higher range of Fe content levels, with the 3rd quartile reaching a value of 1.58 g/100 g compared to a value of 0.97 g/100 g found for the Versailles Plain.

Moreover, coarse fragment content levels in topsoil can reach percentages of as high as 20% and 30% for the 3rd quartile of the Versailles and Peyne sets, respectively.

Table 4. Pearson correlation table of common soil properties for the Versailles Plain

Variables	Clay	Silt	Sand	CaCO3	SOC	Fe	pH	CEC
Clay	**1.00**							
Silt	-0.24	**1.00**						
Sand	**-0.34**	-0.27	**1.00**					
CaCO3	-0.02	**-0.70**	**-0.33**	**1.00**				
SOC	**0.53**	**-0.38**	**-0.44**	**0.46**	**1.00**			
Fe	**0.48**	0.24	0.03	**-0.52**	0.00	**1.00**		
pH	**0.46**	**-0.43**	**-0.50**	**0.60**	**0.66**	-0.25	**1.00**	
CEC	**0.77**	**-0.32**	**-0.52**	**0.33**	**0.82**	0.12	**0.77**	**1.00**

Values in bold are different from 0 at a significance level of alpha=0.05

Table 5. Pearson correlation table of common soil properties of the Peyne Valley

Variables	Clay	Silt	Sand	CaCO3	SOC	Fe	pH	CEC
Clay	**1.00**							
Silt	-0.14	**1.00**						
Sand	**-0.54**	**-0.76**	**1.00**					
CaCO3	-0.08	**0.53**	**-0.40**	**1.00**				
SOC	**-0.19**	0.08	0.06	0.11	**1.00**			
Fe	**0.42**	**-0.26**	-0.06	**-0.50**	-0.11	**1.00**		
pH	0.02	**0.42**	**-0.37**	**0.52**	0.03	**-0.42**	**1.00**	
CEC	**0.89**	-0.16	**-0.45**	0.00	-0.02	0.16	0.14	**1.00**

Values in bold are different from 0 at a significance level of alpha=0.05

For the Versailles Plain, the highest correlations ($|R| > 0.7$) were observed between CEC and SOC content levels, between CEC and clay levels, between CEC and pH levels and between $CaCO_3$ and silt levels (Table 4). Modest correlations ($0.7 > |R| > 0.5$) were observed between pH and SOC levels, between pH and $CaCO_3$ levels, between pH and sand levels, between Iron and $CaCO_3$ levels and between SOC and clay levels (Table 4). For the Peyne catchment, the highest correlations ($|R| > 0.7$) were observed between CEC and clay levels and between sand and silt levels (Table 5). Modest correlations ($0.7 > |R| > 0.5$) were observed between pH and $CaCO_3$ levels, between iron and $CaCO_3$ levels, between sand and clay levels and between silt and $CaCO_3$ levels (Table 5).

4.2 Performance of the prediction models

A PLSR model was built from S2A spectra and from each observed soil property associated with the available soil samples. No spectral outliers were removed from the calibration database, regardless of the study area concerned, and the number of latent variables was determined following the rule of the first local minimum of the RMSECV, which varied between 2 and 9 (Table 6). The predictive capacities of the PLSR models ranged from low to medium to high, with RPD values of between 1.0 and 2.0 and with R^2_{cv} of between 0.02 and 0.75 (Table 6). Three groups of variables can be identified from the cross-validation performance of the PLSR models (Table 6, Fig. 3): i) soil property models yielding $R^2_{cv} \geq 0.5$ and RPD $\geq$1.4 (rounded values) or models with intermediate to high levels of predictability; ii) soil property models with R^2_{cv} and RPD values of 0.4 and 1.3, respectively (rounded values) or models with poor predictive capacities just below thresholds commonly accepted in the literature or 'near intermediate' models; and iii) soil property models with $R^2_{cv} < 0.4$ and RPD values of roughly 1 or models exhibiting poor or very poor levels of predictive capacity.

In overall, the Versailles Plain includes all 4 properties of group i (SOC, pH, CEC and $CaCO_3$) and one property of group ii (Clay), whereas the Peyne region includes 3 properties of group ii (Clay, Iron and CEC), with the remaining properties (silt and sand content for both regions and SOC, pH, and CaCO3 content for the Peyne site) are categorized as group iii.

Table 6. Cross-validation performance statistics derived from the PLSR algorithm for soil property prediction (NL_v, number of latent variables; RMSEcv expressed in original units). R^2_{cv} and RPD rounded values of greater than or equal to 0.5 and 1.4, respectively, are shown in bold (group *i*). RPD rounded values of greater than or equal to 1.3 are shown in italics (group *ii*).

Soil property	Versailles Plain				Peyne Valley			
	R^2cv	RMSEcv	RPD	NL_V	R^2cv	RMSEcv	RPD	NL_V
SOC	**0.56**	1.23	**1.51**	4	0.02	3.71	1.00	4
$CaCO_3$	**0.48**	20.3	**1.39**	4	0.15	122.2	1.08	8
Clay	*0.39*	1.23	*1.30*	6	*0.42*	56.4	*1.31*	5
Silt	0.14	103.0	1.09	3	0.11	91.9	1.06	9
Sand	0.22	81.7	1.14	4	0.03	113.0	1.02	7
Iron content	0.05	0.09	1.02	2	*0.45*	0.04	*1.34*	6
pH	**0.51**	0.51	**1.43**	4	0.08	0.64	1.03	4
CEC	**0.75**	1.23	**2.00**	6	*0.41*	2.41	*1.31*	6

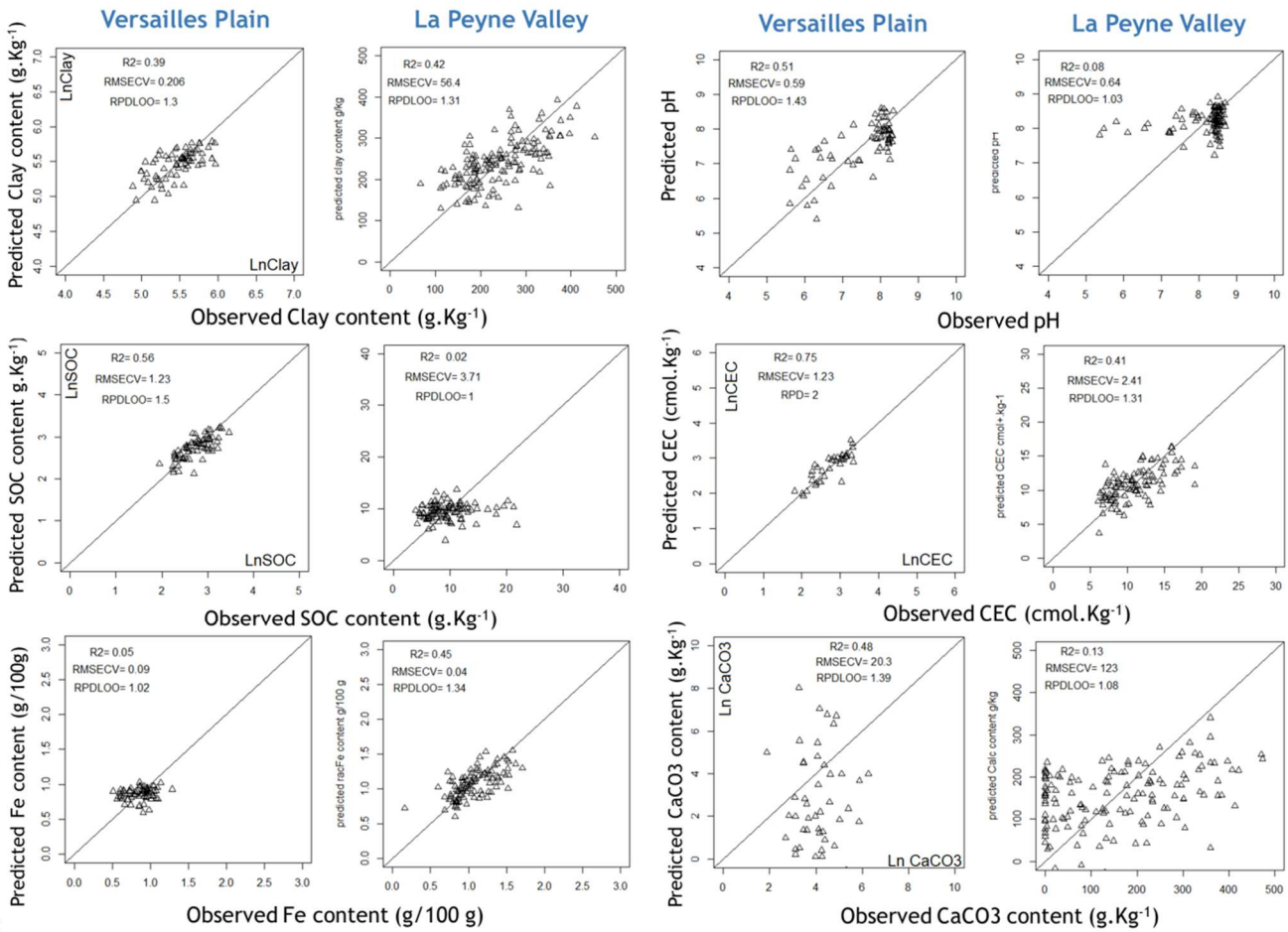

Figure 3. Predicted vs. observed soil properties for the Versailles Plain (left) and Peyne Valley (right) for 6 soil properties best predicted for at least one region

A model property that exhibits intermediate or near intermediate predictive capacity for one region can exhibit poor capacities for another. This is the case for pH, SOC, iron and CaCO3 content levels. A model property that exhibits high predictive capacity for one region can exhibit near intermediate capacities for another: this is the case for CEC levels.

4.3 Soil property mapping from SENTINEL2 data

While retaining PLSR models for groups i and ii, equations were applied to bare cropland and vineyard pixels (Fig. 4).

To relate the output maps to soil data and available soil maps and to facilitate the visual analysis of results for the other maps, and particularly for the Versailles Plain, for which the percentage of mapped pixels is very low, values were simplified to decile classes of predicted bare soil pixels for each study zone (Fig. 4).

The spatial patterns of clay correspond with known soil patterns for both regions. In the Peyne Valley, spatial patterns clearly show chromic luvisols developed along Plio-Quaternary alluvial terraces and characterized by high clay, iron and CEC levels. This result contrasts well with areas with Miocene marine deposits of calcisols and calcaric leptosols with less clay, iron and CEC. However, very high clay and iron content levels predicted for the minor riverbed of the Peyne River (the violet band in the clay map shown in Fig. 4) are not in accordance with our soil knowledge, likely revealing a perturbation related to soil moisture levels.

In the Versailles Plain, the highest predicted clay content levels match our observations of stagnic colluvic cambisols in lower slopes and valleys, whereas the lowest predicted clay content levels as expected were found along the plateaus with luvisols of loess origin. The highest SOC content levels were predicted both for stagnic colluvic cambisols in the valleys and for calcaric cambisols across the slopes, while low SOC content levels were predicted for luvisols originating from loess sources, in accordance with previous studies of the same region (Vaudour et al., 2013, 2016; Zaouche et al, 2017).

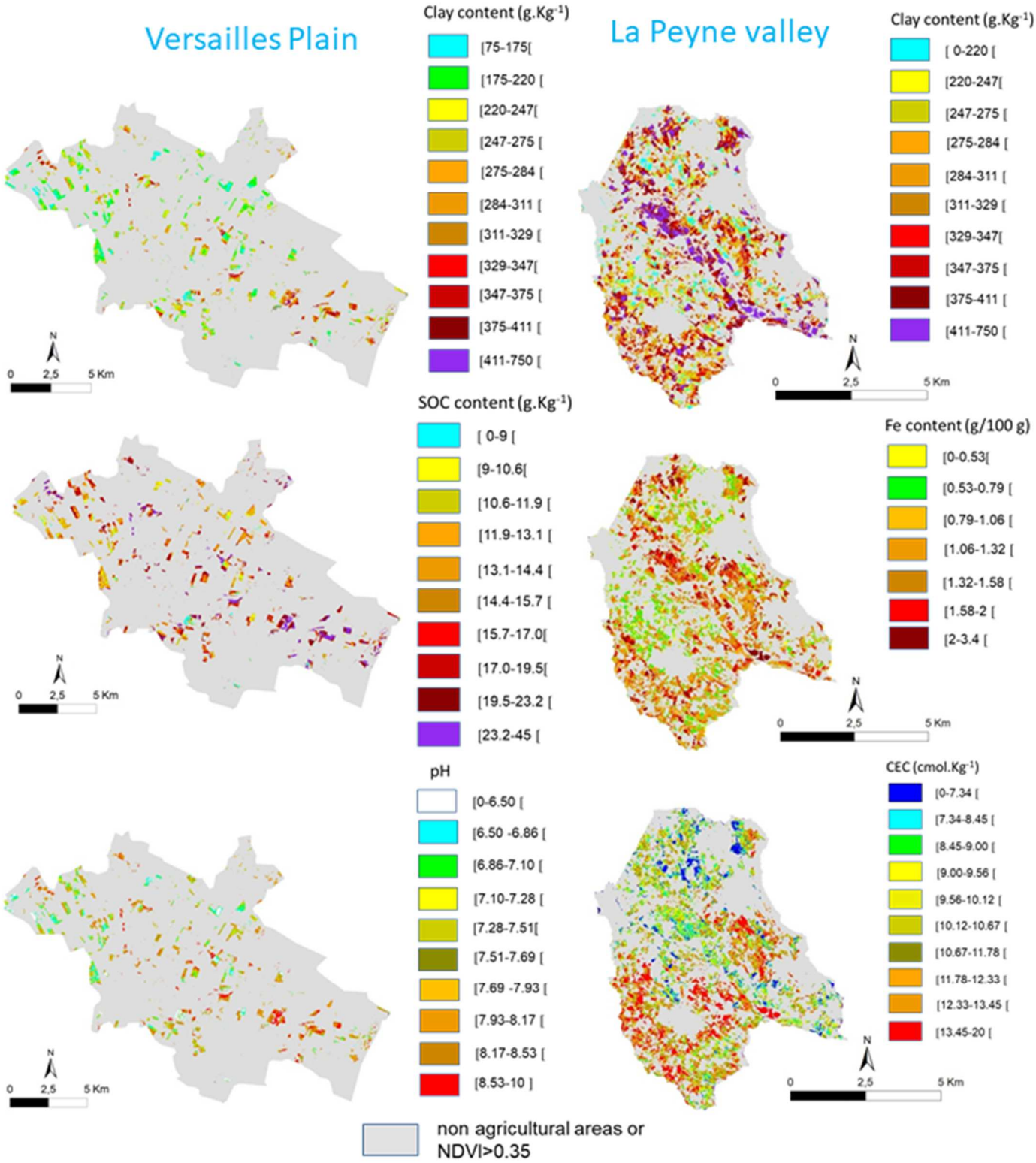

4(

410 Figure 4. Maps of soil properties of the Versailles Plain (left) and Peyne Valley (right)

411

412

413 *4.4 S2A capacities to retrieve spatial structures*

414 *4.4.1 Comparisons between empirical variograms derived from measured and predicted*
415 *values*

416 Following from the map examinations, comparisons drawn between variograms of predicted
417 values of the three best predicted soil properties for the Peyne Valley (clay, Fe, and CEC
418 content, Fig. 5, black curves) and those of measured values for the same locations (Fig. 5 red
419 curves) confirm that the soil patterns are captured by the predictions fairly well. Variograms
420 for clay and CEC are very similar in shape and only show a decrease in the 'nugget' value (at
421 the origin) of the predicted variogram. These differences in variograms have been observed
422 through tests of soil predictions from hyperspectral data (Gomez et al, 2012). The predicted
423 iron variogram has the same nugget and range as the measured one, with only a difference in
424 'sill' values (the slope of the variogram). No clear explanation can be given for this difference
425 in behavior.

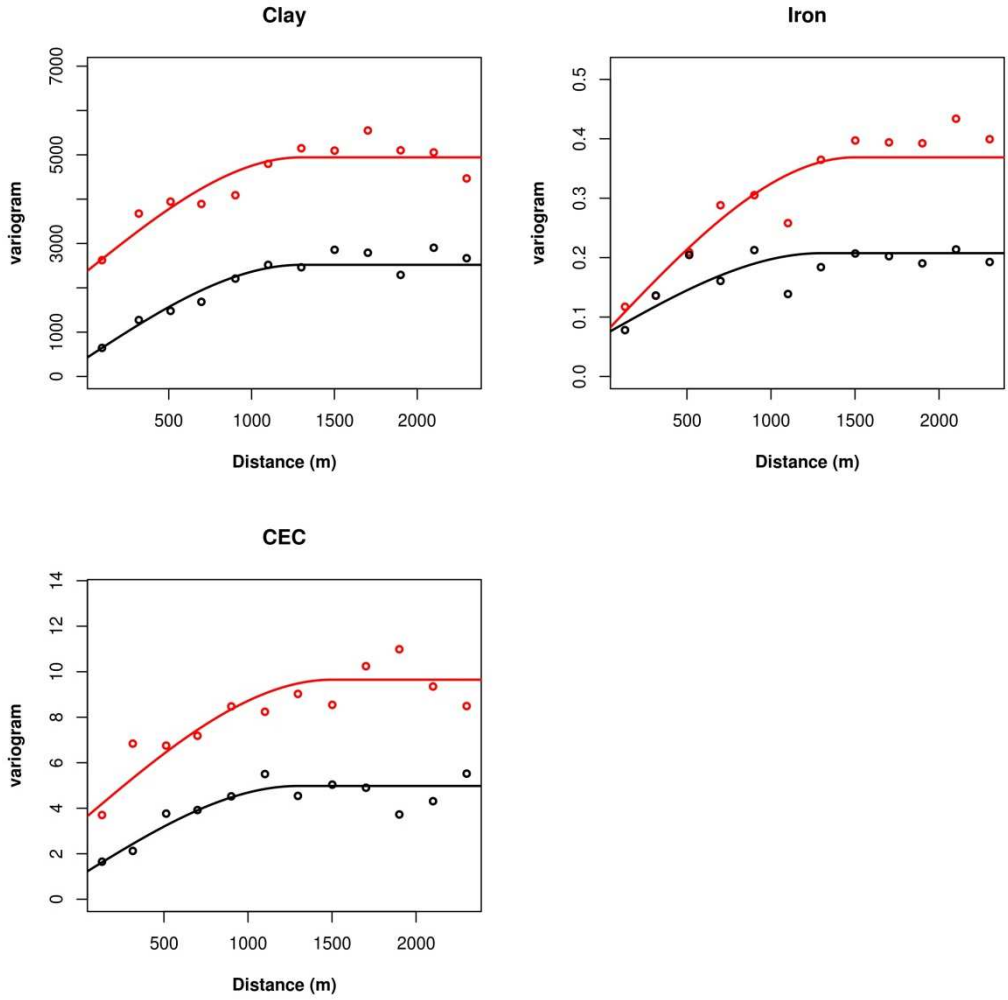

426

427 Figure 5. Empirical variograms calculated for clay, iron and CEC for the Peyne Valley from
428 physico-chemical values of the collected soil samples (red points) and from predicted values
429 based on S2A spectra (black points) and fitted theoretical variograms (lines). Lag = 200 m.
430 Distance max: 2000 m.

431

432 *4.4.2 Spatial structures retrieved from the set of predicted pixels*

433 Empirical variograms were computed from the 46,971 pixels of bare soil in the Peyne
434 catchment (Fig. 6). They exhibit different spatial structures from those revealed by
435 variograms built from the measured sites only (Fig. 5). From an increase in the number of
436 sites tested, short-scale variations are found across the clay and iron variograms as a result of
437 a first slope break at 250 m that is not shown in the previous variograms (Fig. 6). Another

slope break at approximately 1,000 m in the variograms shown in Fig. 6 is still visible but is less pronounced. This more complex spatial structure reveals a combination of soil variations acting at different scales in accordance with our understanding. The broad-scale variability found could be related to the spatial distribution of parent materials of soils with dissimilar clay and iron content levels. Short-range variations may result from erosion-redeposition processes occurring along slopes that involve neighboring parent materials with dissimilar iron and clay content levels.

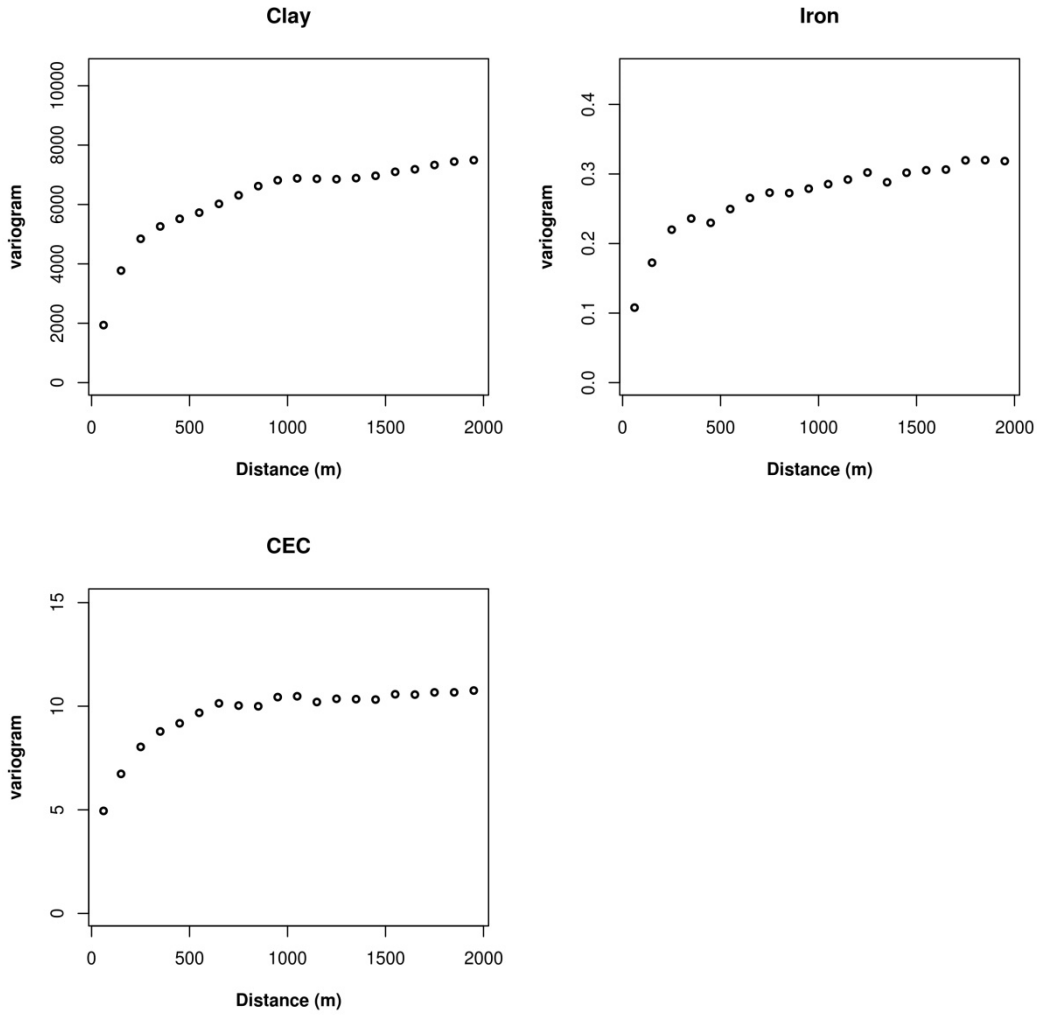

Figure 6. Empirical variograms computed for clay, iron and CEC from predicted soil properties of bare soils of the Peyne. Lag = 100 m. Distance max: 2,000 m.

5. Discussion

5.1 Performance of the S2A-derived PLSR models

Comparisons of the performance of the S2A-derived models for two contrasting agroecosystems suggest that the predictability of a given property does not solely rely on the property itself or particularly on its spectral behavior as a "chromophore" according to Ben Dor et al. (2009). Rather, if such conditions could explain predictive capacities, both iron and SOC content levels would be predicted for any study area, as iron oxides and organic matter are spectrally influent due to their chemical compositions and arrangements, while their specific influent absorption bands are covered by MSI bands. In particular, SOC is known to be spectrally sensitive across the entire VNIR-SWIR spectral range (Ben Dor et al., 2009; Demattê et al., 2015), while the specific absorption wavelengths of iron oxides (550 nm and roughly 860-900 nm) are overlain by green band b3 and near-infrared band b8A. As was expected for SOC, loading values for SOC prediction models were found to be higher overall for the visible b4, b5, near infrared b8A and two SWIR bands (b11, b12) for the Versailles Plain than for the Peyne valley. For iron, loading values were found to be marked for the b3 and b8A bands for the Peyne Valley while they were weakly expressed for the Versailles Plain (Fig. 7). This does not apply for both areas, suggesting that more conditions must be applied to confer predictive capacity. Moreover, clay predictions may be linked to the physical structure of soils in conjunction with a chromophore of approximately 2,200 nm that is fully covered by the b12 band (Table 1): this was revealed by higher loading values (Fig. 7) . However, performance of clay predictionwas only found to be near-intermediate ($0.5 > R^2cv > 0.4$) for both study areas, suggesting that other conditions may hamper predictive capacity levels.

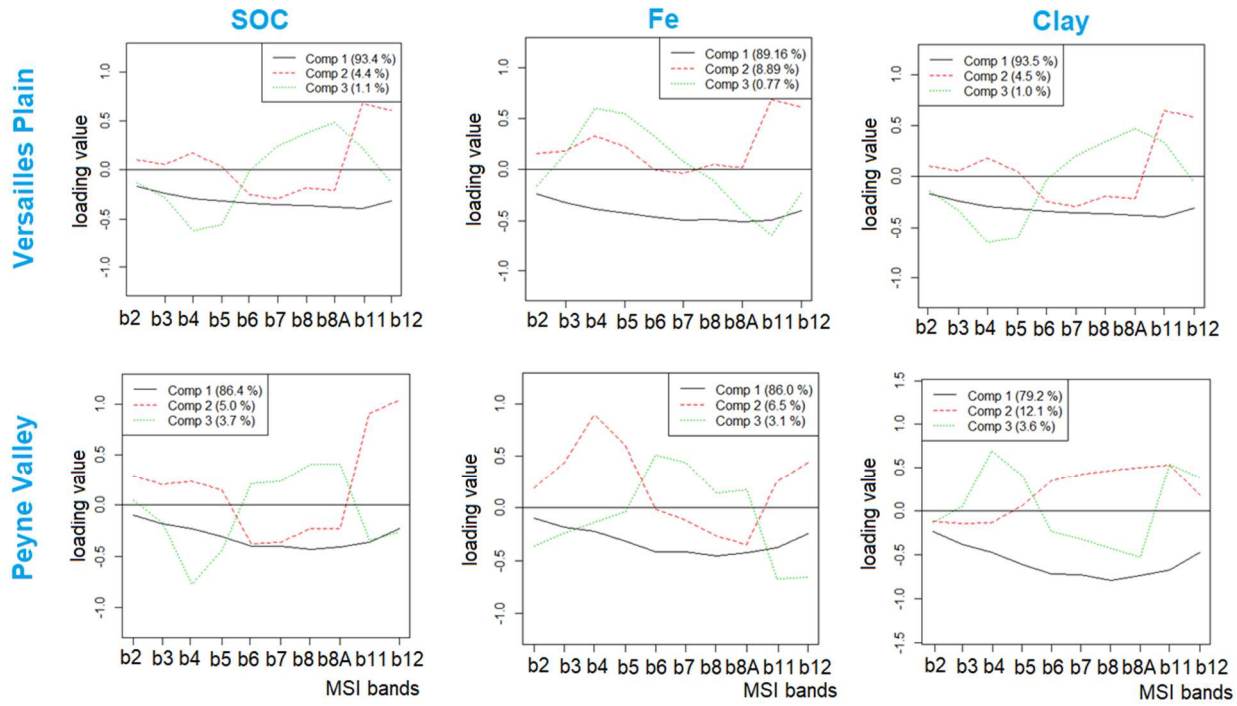

Figure 7. Loading plots for SOC, Fe and Clay of both study areas

First, as previously found by Gomez et al. (2012) for the Peyne Valley, intra-regional variances between the considered properties are large unless considered variables (even when spectrally sensitive) are not predictable. This is the case for both SOC and iron content levels, which are neither abundant nor variable across the Peyne Valley and Versailles Plain, respectively.

Second, if the property considered is correlated with another well-predicted property, this might improve its predictive ability. Performance levels obtained for pH (Versailles Plain) and CEC (Versailles Plain, Peyne Valley) are based on levels of variability across the study regions and correlations to either SOC and/or clay. As a matter of fact, pH and CEC are not spectrally sensitive. Moreover, while $CaCO_3$ has a specific absorption band (2,330 nm), its wavelength is not covered by any MSI band; its predictive ability might therefore be attributed to its correlation to pH (0.6) for the Versailles Plain and other disturbing factors might play a role for the Peyne Valley. Although the prediction model for $CaCO_3$ yielded

intermediate performance figures-of-merit (when rounded) for the Versailles Plain, a careful examination of the PLSR residues suggests that only soils with no or very low $CaCO_3$ content levels present low predictions errors (< 35 $g.kg^{-1}$), and they represent 56% of the dataset, resulting in apparently average intermediate performance (Table 6). Specifically, calcareous soils of the Versailles Plain are as poorly predicted as those of the Peyne Valley. In addition, $CaCO_3$ degrades model accuracy levels for SOC content, as the lab uncertainty of SOC measurements increases with $CaCO_3$ content levels (Vaudour et al., 2016).

Third, the number and composition of sample sets is likely to influence prediction performance. For the Versailles Plain, strong performance recorded for CEC must be considered with caution, as it is based on a small sample size (39 samples) and the model may be overfit.

Fourth, soil surface conditions can be disturbed by soil roughness, soil moisture, emerging and non-covering vegetation, dry vegetation, vine stock and coarse fragment areal coverage. In addition to commonly known difficulties associated with PLSR models in terms of predicting high soil property values (e.g., for SOC (Stevens et al., 2012)), which are inherent to linear models, some additional disturbances can arise from these specific soil surface conditions. As a matter of fact, in the Peyne Valley, higher iron content levels are found among very stony soils with coarse fragment content levels of greater than 40%: the higher the coarse fragment content level, the more significant iron content prediction errors become (Fig. 8). In the Versailles Plain, because calcareous soils are stony and as their rock fragments are made of limestone, such relationships merge with those of calcium carbonate content: the higher the coarse fragment content level, the higher the $CaCO_3$ content level and the higher the SOC content level. The highest levels of $CaCO_3$ content (> 136 g. kg^{-1}) show the highest levels of SOC residue prediction (Fig. 9).

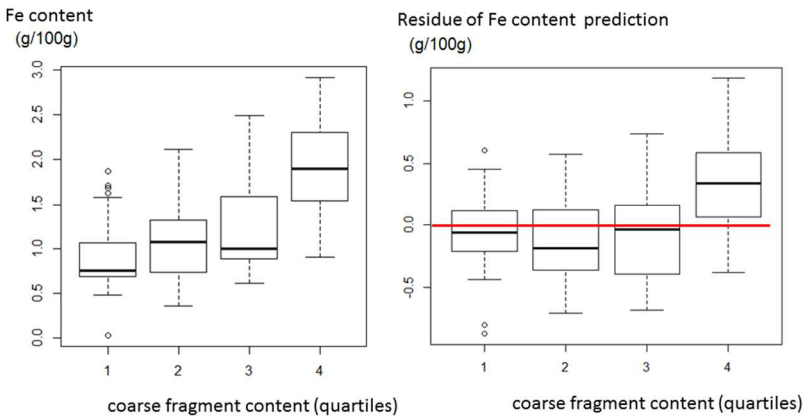

513

514 Figure 8. Relationships between quartiles of coarse fragment content and Fe content (left) and
515 Fe content prediction errors (right) for the Peyne Valley. Quartile thresholds of coarse
516 fragment content: 1, < 7.5%; 2, 7.5-18%; 3, 18-40%; 4, > 40%.

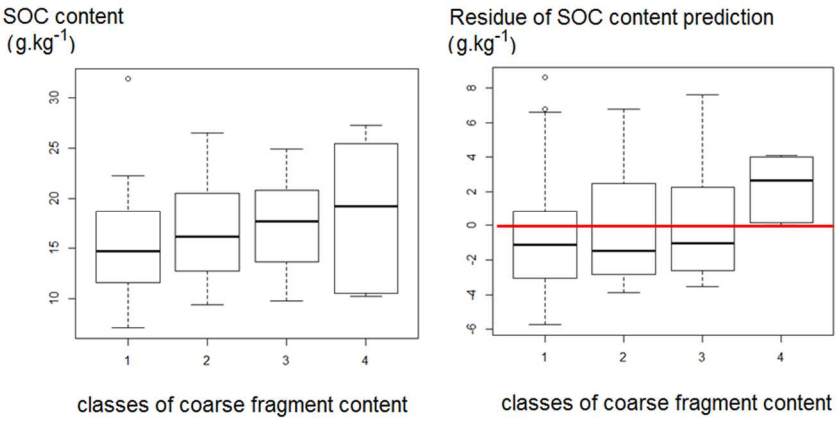

517

518 Figure 9. Relationships between quartiles of coarse fragment content and SOC content (left)
519 and effects of coarse fragment content on SOC content prediction errors (right) for the
520 Versailles Plain. Classes of coarse fragment content: 1, < 7.5%; 2, 7.5-18%; 3, 18-40%; 4, >
521 40%.

Of course, it cannot be inferred from Figs. 8 and 9 that coarse fragment content alone causes prediction errors, but presumably it contributes to such errors.

In terms of vegetation features, the composition and adequacy of the dataset is conditioned by the NDVI threshold. Regarding dry vegetation, while the b12 band covers the 2,100 nm specific absorption wavelength for cellulose (Daughtry 2001), the MSI bands do not enable one to derive an index of dry vegetation such as the Cellulose Absorption Index (CAI = 0.5 ($R_{2000\ nm}$+$R_{2200\ nm}$)-$R_{2100\ nm}$) elaborated by Nagler et al. (2000). The CAI relies on two wavelengths covered by the b12 band (2,100 and 2,200 nm), but it requires the use of the 2,000 nm wavelength not covered by any MSI band. However, other indexes, such as the Normalized Difference Tillage Index defined for Landsat Thematic Mapper (TM) bands (NDTI= (TM5-TM7)/(TM5+TM7)) (Van Deventer et al., 1997), could be adapted and tested for discriminating crop residue cover. The S2A data thus show limits in accounting for crop residue cover and vine wood vegetation more than the MSI spatial resolution does not enable one to discriminate between vine rows and vine interrows to remove the spectral influence of vine woods.

In conclusion, our use of two contrasting agroecosystems datasets denotes what is achievable from S2A data in terms of predictive capacities for a single considered date. The soils considered in this study are located in French regions but widely develop abroad, across the temperate and Mediterranean areas. Assessment of Sentinel-2 performance is developing for other French regions with other soil types and further for tropical soils.

547

548 *5.2 Comparisons with other sensors*

549 Our model performs in a similar manner as those employed in other studies. It
550 performs better than SPOT multispectral satellite images in measuring SOC, and it performs
551 similarly or less optimally than hyperspectral airborne images in measuring all properties.

552 For the Versailles Plain in particular, previous models of SOC content were derived
553 from multispectral or hyperspectral fields or from image spectra. In terms of RMSECV and
554 RPD values in particular, the regional PLSR model obtained SOC content levels from S2A
555 spectra (1.23 $g.kg^{-1}$ and 1.51, respectively) more accurately than real SPOT or simulated
556 SPOT spectra (Vaudour et al., 2013: error range 4.5-6.0 $g.kg^{-1}$, RPD 0.9-1.3) for the same
557 region. This is presumably attributable to the beneficial role of its SWIR bands and to
558 differences in soil surface conditions, which are similar to those obtained from a VNIR
559 hyperspectral AISA airborne image (no SWIR) for the same region (Vaudour et al., 2016:
560 error range 2.82-3.79 $g.kg^{-1}$, RPD 1.3-1.6).

561 For the Peyne Valley, performance outcomes obtained from Sentinel-2 are lower
562 than those obtained from a VNIR-SWIR Hymap airborne image (Gomez et al., 2012),
563 regardless of soil properties involved with dramatic changes in performance found for $CaCO_3$
564 content effectively predicted from the hyperspectral spectra but not predicted from S2A
565 spectra (see §5.1). However, due to intra-regional variances (SOC) and an absence of
566 correlations with more effectively predicted properties (silt), neither SOC nor silt content
567 levels were predicted from hyperspectral and S2A images. Performance degradation from
568 airborne to spaceborne models has also been found by Steinberg et al. (2016) for SOC, clay
569 and iron content levels, though these authors used simulated EnMAP satellite spectra.

570 It must be noted that our models were constructed from actual spaceborne images that
571 account for the effects of atmospheric, signal/noise ratio, and soil surface conditions and

notably coarse fragment content and vegetation. This distinguishes our models from those constructed from simulated MSI spectra derived from lab spectral libraries, as anticipated by Castaldi et al. (2016) for a number of forthcoming or newly launched satellites, including Sentinel-2. However, with the addition of noise and atmospheric effects and from the use of untransformed lab reflectance spectra sampled from central and southern Italy, these authors obtained validation results similar to our performance results for clay (R^2 0.36-0.42; RPD 1.26-1.35) that are inferior to those found for the Versailles Plain in terms of SOC content levels (R^2 0.36; RPD 1.26) in the best case or that are not as predictive as found for the Peyne (R^2 0.13; RPD 1.09) in the worst case. Gomez et al. (2018) used VNIR/SWIR hyperspectral airborne data (initial spectral resolution of approximately 5 nm) to simulate, among others, Sentinel-2, Landsat 8 and Landsat 7 spectral resolution data. They showed that these multispectral sensors provide very modest performances of clay content estimations, as these spectral resolutions do not provide clay absorption feature useful in regression models.

5.3 M*aximizing the mapped area*

As the presence of vegetation severely hampers the prediction of soil properties from VNIR/SWIR remote sensing data, it is important to retrieve as many bare soil signals as possible. When only one image is considered, as was done in this study, this involves a careful selection of acquisition periods. Images of the Versailles Plain and Peyne Valley were acquired for the spring period to maximize the size of the area with bare soils. In temperate agroecosystems like that of the Versailles Plain, this corresponds to the sowing of spring cereals, with the winter period being less suitable due to impacts of the Nitrate Directive that requires intermediate crop cultivation (Vaudour et al., 2013). In a Mediterranean agroecosystem like that of the Peyne Valley, the spring period corresponds to maximum tilled vineyard coverage for removing weeds (Paré, 2007) while green vegetation is not yet present.

597 Despite this careful selection of periods, coverage levels found for bare soil areas remain
598 modest, especially for the Versailles Plain (Fig. 4).

599 Bare soil areas could be maximized (at least for temperate agroecosystems) by
600 aggregating multiple acquisition dates. This would allow one to accumulate the spectra of soil
601 areas that change every year and along the crop cycle. Sentinel-2 is particularly well suited to
602 this task, as it provides an image every 5 days, thus increasing the likelihood of acquiring
603 images under clear conditions and across the crop rotation cycle.

604 Such an aggregation of images for maximizing bare soil areas was already attempted
605 by Diek et al. (2016). These authors doubled the bare soil area by combining hyperspectral
606 APEX acquisitions over 3 successive years and performed intercalibration from linear
607 regressions of atmospherically corrected spectra for different years. This raises issues relating
608 to accurate atmospheric corrections across dates and to the number and anteriority values of
609 dates. This issue is being studied in reference to the Versailles Plain to consider the
610 directional effects of soil roughness in line with tillage operations (Vaudour et al., 2014a).
611 Indeed, soil roughness levels can be spatially and temporally retrieved from optical/radar
612 pairs such as S2/S1 (Vaudour et al., 2014b), which could be accounted for during soil
613 properties prediction.

614 Bare soil coverage levels can also be increased by applying unmixing techniques that
615 isolate bare soil signals from semi-vegetated pixels (Bartholomeus et al 2011, Ouerghemmi et
616 al., 2016). For the Peyne Valley, such techniques are used to predict clay content levels from
617 hyperspectral data for semi-vegetated areas (NDVI < 0.55), expanding the studied surface
618 from 4% (bare soil) to 63% of the total area (Ouerghemmi et al., 2016). A similar approach
619 could be applied for S2A soil predictions.

620

621

622

623 *5.4. Incorporating S2A data into the framework of digital soil mapping*

624 The soil predictions obtained from S2A are neither precise nor extended enough to be
625 exploited "as is" by end users. They must rather be considered as a new source of soil data
626 that should be used for Digital Soil Mapping (Mc Bratney et al, 2003, Lagacherie et al, 2007),
627 a larger methodological framework that can produce more exhaustive and precise soil maps.
628 If we examine the soil property predictions obtained in this study with such a perspective in
629 mind, S2A soil predictions obtained from this study could serve as valuable inputs for digital
630 soil mapping for two reasons.
631 First, S2A data offer insight on the spatial patterns of certain soil properties that could be
632 quantified from variograms that closely resemble those obtained from real measurements.
633 These variograms could be used to optimize further sampling efforts, as they allow one to
634 compute error variances (kriging variance) for sampling schemes of different densities and
635 spatial distributions and thus determine the sampling efforts required to meet target levels of
636 precision in spatial predictions (McBratney et al., 1981).
637 Second, S2A products could serve as surrogate data to improve the precision of Digital Soil
638 Mapping models (Lagacherie & Gomez; 2013). For example, Walker et al. (2017) found the
639 use of hyperspectral data as soft data for co-kriging or cogriging with external drift models to
640 improve prediction performance. Although less pronounced, improvements were still
641 observable when using hyperspectral-based estimations of moderate quality ($R^2 < 0.5$) like
642 many of those obtained in this study. It is therefore expected that some S2A soil outputs could
643 make improvements while being more available than hyperspectral data.
644 Finally, the potential of S2 data as a co-variable in DSM model could further be evaluated.
645 While previous researches used MODIS or LANDSAT data in DSM models, either as
646 spectral indexes, such as the NDVI (e.g., Mishra et al., 2010), or as spectral bands (e.g., Were

et al., 2015). Zaouche et al (2018) found improvement incorporating the green band of SPOT into a joint Bayesian model, and development of their approach is in progress for Sentinel2.

6. Conclusion

S2A image spectra acquired from two French study areas representative of temperate and Mediterranean agroecosystems—the Versailles Plain and the Peyne Valley—were tested as input data of a chemometric model (PLSR) to predict 8 topsoil properties of bare soil areas: 8% and 39% of the Versailles Plain and the Peyne Valley, respectively. Six of these 8 soil properties (clay, SOC, iron, $CaCO_3$, pH, and CEC levels) can be predicted with varying success depending on their intrinsic spectral properties, intra-regional variances, correlations and soil surface conditions. Some of the best predictions were also found to serve as good approximations of the spatial patterns of soil properties.

Although a significant decline in the prediction performance of those obtained from hyperspectral data for the same study areas was observed, S2A soil predictions can serve as valuable inputs for Digital Soil Mapping. With the current absence of efficient hyperspectral satellites that can deliver hyperspectral data, it is advantageous to allow for the mosaicking of multidate acquisition and for the selection of the best acquisitions over a time series. We therefore recommend their use to improve the performance of Digital Soil mapping predictions.

Acknowledgment

This study was carried out in the framework of the TOSCA “Cartographie Numérique des Sols (CNS)” program of the French Space Agency (CNES). It also benefited support from the TOSCA-PLEIADES-CO program of the CNES for the Versailles Plain. Special thanks to Dalila Hadjar, Arthur Scriban, Paulina Michura, for technical assistance in the field. We are

also indebted to Yves Blanca, IRD-UMR LISAH Montpellier, for the soil samples sampling in 2009 over the vineyard Plain of Languedoc.

References

AFNOR, 1999. Qualité des sols. AFNOR, Paris, vol. 1, 565 p. (in French)

Adeline K., Gomez C., Gorretta N., Roger J.M., 2017. Predictive ability of soil properties to spectral degradation from laboratory Vis-NIR spectroscopy data. Geoderma. 288, pp. 143–153.

Adhikari, K., Hartemink, A.E., 2016. Linking soils to ecosystem services - a global review. Geoderma 262, 101–111.

Arrouays, D., Grundy, M.G., Hartemink, A.E., Hempel, J.W., Heuvelink, G.B.M., Young Hong, S., Lagacherie, P., Lelyk, G., McBratney, A.B., McKenzie, N.J., Mendonça-Santos, M.L., Minasny, B., Montanarella, L., Odeh, I.O.A., Sanchez, P.A., Thompson, J.A., Zhang, G.L., 2014. GlobalSoilMap: toward a fine-resolution global grid of soil properties. Advances in Agronomy, 125, 93-134.

Arrouays, D., Lagacherie, P., Hartemink, A.E., 2017. Digital soil mapping across the globe. Geoderma Reg. 9, 1–4.

Bartholomeus, H., Kooistra, L., Stevens, A., Leeuwen, M., Wesemael, B., Ben-Dor, E., Tychon, B., 2011. Soil organic carbon mapping of partially vegetated agricultural fields with imaging spectroscopy. International Journal of Applied Earth Observation and Geoinformation 13 (1), 81–88.

Baveye, P., Baveye, J., Gowdy, J., 2016. Soil “ecosystem” services and natural capital: critical appraisal of research on uncertain ground. Frontiers in Environmental Science, 4 (41).

696 Ben-Dor, E., Chabrillat, S., Demattê, J.A.M., Taylor, G.R., Hill, J., Whiting, M.L., Sommer,
697 S., 2009. Using imaging spectroscopy to study soil properties. Remote Sens. Environ.
698 113, S38-S55.

699 Castaldi, F., Palombo, A., Santini, S., Pignatti, S., Casa, R., 2016. Evaluation of the potential
700 of the current and forthcoming multispectral and hyperspectral imagers to estimate soil
701 texture and organic carbon. Remote Sensing of Environment, 179, 54-65.

702 Chang, C.W., Laird, D.A., Mausbach, M.J., Hurburgh, C.R., 2001. Near infrared reflectance
703 spectroscopy: principal components regression analysis of soil properties. Soil Sci. Soc.
704 Am. J. 65, 480-490.

705 Crahet, M., 1992. Soil Map of the Versailles Plain. Scale 1:50 000. Institut National
706 Agronomique Paris-Grignon, Grignon, Internal report.

707 Daughtry, C.S.T., 2001. Discriminating crop residues from soil by shortwave infrared
708 reflectance. Agron. J. 93, 125-131.

709 Demattê; J., Morgan, C.L.S. Chabrillat, S., Rizzo, R., Franceschini, M.H.D., Terra, F.daS.,·
710 Vasques, G.M., Wetterlind J., 2015. Spectral sensing from ground to space in soil
711 science: State of the art, applications, potential and perspectives. In book: Remote
712 Sensing Handbook - Land Resources Monitoring, Modeling, and Mapping with Remote
713 Sensing, Publisher: CRC Press, Editors: P.S. Thenkabail, pp.661-732.

714 Diek, S., Schaepman, M.E., de Jong, R., 2016. Creating Multi-Temporal Composites of
715 Airborne Imaging Spectroscopy Data in Support of Digital Soil Mapping. Remote Sens.
716 8, 906.

717 Filzmoser, P., Garrett, R.G., Reimann, C., 2005. Multivariate outlier detection in exploration
718 geochemistry. Computers&Geosciences 31, 579-587.

719 Folkman, M., Pearlman, J., Liao, L., Jarecke, P., 2001. EO1/Hyperion hyperspectral imager
720 design, development, characterization and prediction. In: Smith, W.L., Yasuoka, Y.
721 (Eds.), Hyperspectral Remote Sensing of the Land and Atmosphere. SPIE Proceeding,
722 vol. 4151, pp. 40–51.

723 Geladi, P., Kowalski, B. R., 1986. Partial least squares regression: a tutorial. Analytica
724 Chimica Acta 185, 1-17.

725 Gomez, C, Adeline, K., Bacha, S., Driessen, B., Gorretta, N, Lagacherie, P, Roger, JM,
726 Briottet, X., 2018. Sensitivity of clay content prediction to spectral configuration of
727 VNIR/SWIR imaging data, from multispectral to hyperspectral scenarios. Remote
728 Sensing of Environment 204, 18-30.

729 Gomez, C., Viscarra Rossel, R.A., McBratney, A.B., 2008. Soil organic carbon prediction by
730 hyperspectral remote sensing and field vis-NIR spectroscopy: an Australian case study.
731 Geoderma 146, 403–411.

732 Gomez, C., Coulouma, G., Lagacherie, P., 2012a. Regional predictions of eight common soil
733 properties and their spatial structures from hyperspectral Vis–NIR data, Geoderma,
734 189–190, 176-185.

735 Gomez, C., Lagacherie P., Bacha, S., 2012b. Using an VNIR/SWIR hyperspectral image to
736 map topsoil properties over bare soil surfaces in the Cap Bon region (Tunisia). In
737 “Digital Soil Assessments and Beyond”Minasny B., Malone B.P., McBratney A.B.
738 (Ed.).Springer, 387-392.

739 Gomez, C., Oltra-Carrió, R., Bacha, S., Lagacherie, P., Briottet, X., 2015. Evaluating the
740 sensitivity of clay content prediction to atmospheric effects and degradation of image
741 spatial resolution using hyperspectral VNIR/SWIR imagery. Remote Sens. Environ.
742 164, 1-15.

743 Goovaerts, P., 1997. Geostatistics for natural resources evaluation. Oxford University Press,
744 New York.
745 Hagolle, O., 2013. Séries temporelles, SPOT4 Take Five blog, URL: http://www.cesbio.ups-
746 tlse.fr/multitemp/
747 Hagolle, O., Huc, M., Villa Pascual, D., Dedieu, G., 2010. A multi-temporal method for cloud
748 detection, applied to FORMOSAT-2, VENμS, LANDSAT and SENTINEL-2 images.
749 Remote Sens. Environ. 114, 1747-1755.
750 Kennard R. W., Stone L. A., 1969. Computer aided design of experiments. Technometrics 11,
751 1, 137–148.
752 Lagacherie, P., Sneep, A.-R., Gomez, C., Bacha, S., Coulouma, G., Hamrouni, M.H., Mekki,
753 I., 2013. Combining Vis–NIR hyperspectral imagery and legacy measured soil profiles
754 to map subsurface soil properties in a Mediterranean area (Cap-Bon, Tunisia).
755 Geoderma 209–210, 168–176.
756 Mark, H.L., Tunnell, D., 1985. Qualitative near-infrared reflectance analysis using
757 Mahalanobis distances. Anal. Chem. 57, 1449-1456.
758 McBratney, A. B., Webster, R., Burgess, T. M.: The design of optimal sampling schemes for
759 local estimation and mapping of regionalized variables. I. Theory and Method,
760 Computers and Geosciences, 7, 331–334, 1981.
761 McBratney, A.B., Mendonca Santos, M.L., Minasny, B., 2003. On digital soil mapping.
762 Geoderma 117, 3–52.
763 Mehra O.P., Jackson M.L., 1960. Iron oxide removal from soils and clays by a dithionite-
764 citrate system buffered with sodium bicarbonate. In Clays and Clay Minerals;
765 Proceedings of the 7th Conference, Nat1 Acad. Sci-Nat1 Res. Council Publ.,
766 Washington, DC, pp. 317-327.

767 Mevik B.H., Wehrens R., 2007. The pls package: principal component and partial least
768 squares regression in R. Journal of Statistical Software 18, 2, 1-24.
769 Minasny, B., McBratney, A.B., 2016. Digital soil mapping: A brief history and some lessons.
770 Geoderma 264, 301–311.
771 Nagler, P.L., Daughtry, C.S.T., Goward, S.N., 2000. Plant litter and soil reflectance. Remote
772 Sens. Environ. 71, 207-215.
773 Mishra, U., Lal, R., Liu, D., Van Meirvenne, M., 2010. Predicting the Spatial Variation of the
774 Soil Organic Carbon Pool at a Regional Scale. Soil Science Society of America Journal
775 74, 906. https://doi.org/10.2136/sssaj2009.0158
776 Ouerghemmi, W., Gomez, C., Naceur, S., Lagacherie, P., 2016. Semi-blind source separation
777 for the estimation of the clay content over semi-vegetated areas using VNIR/SWIR
778 hyperspectral airborne data. Remote Sens. Environ. 181, 251–263.
779 Paré, N., 2007. Etude de la variabilité et de la dynamique des états de surface des sols
780 viticoles méditerranéens. Master Thesis AgroParisTech Paris.
781 Pebesma, E.J., 2004. Multivariable geostatistics in S: the gstat package. Comput. Geosci. 30,
782 683–691.
783 R Development Core Team, 2015. The Comprehensive R Archive Network. The R
784 Foundation for Statistical Computing, Wirtschaft Universitat, Vienna, Austria. URL:
785 http://www.r-project.org/
786 Ramirez-Lopez, L., Schmidt, K., Behrens, T., Van Wesemael, B., Demattê, J.A.M., Scholten,
787 T., 2014. Sampling optimal calibration sets in soil infrared spectroscopy. Geoderma
788 226-227, 140-150.
789 Richter, R., Schläpfer, D., 2016. ATCOR2/3 User guide, v.9.0.2, March 2016, 263 p.

790 Sanchez, P.A., Ahamed, S., Carré, F., Hartemink, A.E., Hempel, J., Huising, J., Lagacherie,
791 P., McBratney, A.B., McKenzie, N.J., Mendonca Santos, M.L., Minasny, B.,
792 Montanarella, L., Okoth, P., Palm, C.A., Sachs, J.D., Shepherd, K.D., Vågen, T.-G.,
793 Vanlauwe, B., Walsh, M.G., Winowiecki, L.A., Zhang, G.-L., 2009. Environmental
794 science. Digital soil map of the world. Science 325, 680–1.

795 Selige, T., Böhner, J., Schmidhalter, U., 2006. High resolution topsoil mapping using
796 hyperspectral image and field data in multivariate regression modeling procedures.
797 Geoderma 136, 235–244. https://doi.org/10.1016/j.geoderma.2006.03.050

798 Shabou, M., Mougenot, B., Chabaane, Z.L., Walter, C., Boulet, G., Aissa, N.B. Zribi, M.
799 2015. Soil Clay Content Mapping Using a Time Series of Landsat TM Data in Semi-
800 Arid Lands. Remote Sensing. 7, 6059-6078.

801 Steinberg, A., Chabrillat, S., Stevens, A., Segl, K., Foerster, S., 2016. Prediction of common
802 surface soil properties based on Vis-NIR airborne and simulated EnMAP impaging
803 spectroscopy data: prediction accuracy and influence of spatial resolution. Remote
804 Sensing, 8, 613. Doi:10.3390/rs8070613

805 Stevens, A., Miralles, I., Van Wesemael, B., 2012. Soil organic carbon predictions by
806 airborne imaging spectroscopy: comparing cross-validation and validation. Soil Sci.
807 Soc. Am. J. 76, 2174-2183.

808 Stevens, A., Udelhoeven, T., Denis, A., Tychon, B., Lioy, R., Hoffman, L., Van Wesemael,
809 B., 2010. Measuring soil organic carbon in croplands at regional scale using airborne
810 imaging spectroscopy. Geoderma 158, 32-45.

811 Van Deventer, A.P., Ward, A.D., Gowda, P.H., Lyon, J.G., 1997. Using Thematic Mapper
812 data to identify contrasting soil plains and tillage practices. Photogrammetric
813 Engineering & Remote Sensing 63, 1, 87-93.

814 Vaudour, E., Bel, L., Gilliot, J.M., Coquet, Y., Hadjar, D., Cambier, P., Michelin, J., Houot,
815 S., 2013. Potential of SPOT multispectral satellite images for mapping topsoil organic
816 carbon content over peri-urban croplands. Soil Sci. Soc. Am. J. 77, 2122-2139.

817 Vaudour, E., Gilliot, J.M., Bel, L., Bréchet, L., Hadjar, D., Hamiache, J., Lemonnier, Y.,
818 2014a. Uncertainty of soil reflectance retrieval from SPOT and RapidEye multispectral
819 satellite images using a per-pixel bootstrapped empirical line atmospheric correction
820 over an agricultural region. International Journal of Applied Earth Observation and
821 Geoinformation 26, 217-234.

822 Vaudour, E., Baghdadi, N., Gilliot, J.M., 2014b. Mapping tillage operations over a peri-urban
823 region using combined SPOT4 and ASAR/ENVISAT images. Int. J. Appl. Earth
824 Observ.Geoinf. 28, 43-59.

825 Vaudour, E., Gilliot, J.M., Bel, L., Lefevre, J., Chehdi, K., 2016. Regional prediction of soil
826 organic carbon content over temperate croplands using visible near-infrared airborne
827 hyperspectral imagery and synchronous field spectra. Int. J. Appl. Earth Observ.Geoinf.
828 49, 24-38.

829 Vaudour, E., Noirot-Cosson, P.E., Membrive, O., 2015. Early-season mapping of crops and
830 cultural operations using very high spatial resolution Pléiades images. Int. J. Appl. Earth
831 Observ.Geoinf. 42, 128-141.

832 Wold, S., Sjöström, M., Eriksson, L., 2001. PLS-regression: a basic tool of chemometrics.
833 Chemometrics and Intelligent Laboratory Systems 58, 109-130.

834 World Reference Base (WRB), 2014. World reference base for soil resources. A framework
835 for international classification, correlation and communication. Food and Agriculture
836 Organization of the United Nations, Rome, 128 p.

837 Zaouche, M., Bel, L., Vaudour, E., 2017. Geostatistical mapping of topsoil organic carbon
838 and uncertainty assessment in Western Paris croplands (France). Geoderma Regional
839 10, 126-137.

840 Were, K., Bui, D.T., Dick, Ø.B., Singh, B.R., 2015. A comparative assessment of support
841 vector regression, artificial neural networks, and random forests for predicting and
842 mapping soil organic carbon stocks across an Afromontane landscape. Ecological
843 Indicators 52, 394–403. https://doi.org/10.1016/j.ecolind.2014.12.028

844 Zaouche, M., Bel, L., Tressou, J., Vaudour, E., 2018. Soil organic carbon modelling using
845 jointly different sources. METMA2018, Montpellier (France), poster.
846 http://metma2018.sfds.asso.fr/assets/Download/proceedingsMETMA9.pdf

847 **List of figure captions**

848 Figure 1. Locations of soil samples from the Versailles Plain (left, infrared colored S2A
849 image from 12 March 2016) and the lower Peyne Valley (right, infrared colored S2A image
850 from 19 March 2016), ©ESA 2016

851 Figure 2. Selection of reflectance image spectra covering the whole dataset reflectance range
852 and the main soil types

853 Figure 3. Predicted vs. observed soil properties for the Versailles Plain (left) and Peyne
854 Valley (right) for 6 soil properties best predicted for at least one region

855 Figure 4. Maps of soil properties of the Versailles Plain (left) and Peyne Valley (right)

856 Figure 5. Empirical variograms calculated for clay, iron and CEC for the Peyne Valley from
857 physico-chemical values of the collected soil samples (red points) and from predicted values
858 based on S2A spectra (black points) and fitted theoretical variograms (lines). Lag = 200 m.
859 Distance max: 2000 m.

860 Figure 6. Empirical variograms computed for clay, iron and CEC from predicted soil
861 properties of bare soils of the Peyne. Lag = 100 m. Distance max: 2,000 m.

862 Figure 7. Loading plots for SOC, Fe and Clay of both study areas

863 Figure 8. Relationships between quartiles of coarse fragment content and Fe content (left) and
864 Fe content prediction errors (right) for the Peyne Valley. Quartile thresholds of coarse
865 fragment content: 1, < 7.5%; 2, 7.5-18%; 3, 18-40%; 4, > 40%.

866 Figure 9. Relationships between quartiles of coarse fragment content and SOC content (left)
867 and effects of coarse fragment content on SOC content prediction errors (right) for the
868 Versailles Plain. Classes of coarse fragment content: 1, < 7.5%; 2, 7.5-18%; 3, 18-40%; 4, >
869 40%.

870